Sediment recycling at the slab-mantle interface andfore-arc metasomatism: experimental production ofK-rich metasomes

Fatma Gülmez
Istanbul Technical University
Dejan Prelević (prelevic@uni-mainz.de)
Johannes Gutenberg University of Mainz
Michael W. Förster
Macquarie University
Stephan Buhre
Johannes Gutenberg University of Mainz
Jennifer Günther
Johannes Gutenberg University of Mainz

Article

Keywords:

Posted Date: May 22nd, 2023

DOI: https://doi.org/10.21203/rs.3.rs-2929095/v1

Additional Declarations: No competing interests reported.

Version of Record: A version of this preprint was published at Scientific Reports on November 10th, 2023.
See the published version at https://doi.org/10.1038/s41598-023-46367-7.

Sediment recycling at the slab-mantle interface and fore-arc metasomatism: experimental production of K-rich metasomes

Fatma Gülmez[1], Dejan Prelević[2,3*], Michael W. Förster[4], Stephan Buhre[3], and Jennifer Günther[3]

[1]Department of Geological Engineering, Istanbul Technical University, 34469 İstanbul, Turkey
[2]University of Belgrade, Faculty of Mining and Geology, ⁻Dušina 7, 11000 Belgrade, Serbia
[3]Institut für Geowissenschaften, Johannes-Gutenberg-Universität, 55099 Mainz, Germany
[4]School of Natural Sciences, Macquarie University, NSW 2109, Sydney
[*]prelevic@uni-mainz.de

ABSTRACT

Sediment contribution to the mantle is the key step for the generation of orogenic magmatism to produce its isotopic and geochemical inventory. Even though they are exceptional for the subduction settings, there are worldwide samples of arc related ultrapotassic mafic magmas which require complex multi-stage processes along with sediment melting. To understand the metasomatism leading the mantle to produce ultrapotassic mafic melts we simulated the reactions of depleted (harzburgite) and fertile (lherzolite) mantle with subducted carbonate-rich sediment at relatively cold (800-850 °C) and shallow (2 GPa, 60-80 km) slab-mantle interfaces. The progressive devolatilization of the sediments can trigger the formation of immiscible and conjugate carbonatitic and silicic melts which flux the mantle to develop exotic minerals and dolomitic melts. The metasomatic growth product is a wehrlite composed of clinopyroxene, phlogopite, carbonate minerals, and amphibole.

Introduction

Sediment recycling within the mantle wedge contributes considerably to the geochemistry of arc magmas. In orogens like the Alpine-Himalayan orogenic belt **(AHOB)**, this recycling is not only essential for the composition of the arc volcanism, but also forms metasomatic domains within the lithospheric mantle, so-called metasomes which will be stored and activated after active-margin processes have ceased, that is, during subsequent post-collisional ultrapotassic magmatism[1,2]. Carbonates and silicates are major constituents of the sediment load of the subducting column, and their devolatilization and melting represent a principal source of fluids and/or melts that will metasomatize the overriding mantle[3]. By interaction of the mantle with hydrous silicate melts, aqueous fluids and supercritical siliceous, carbonatitic, and alkaline solutions, the metasomes will be ultimately produced ([4–7]).

The metasomatic effects of the recycling of silicate- and carbonate-rich sediments on the mantle-wedge are distinct: recycling of siliciclastic sediments will result in enrichment in silica with potassium and depletion in HFSEs relative to LILE whereas it is expected that the carbonate-rich sediments will lead to extreme silica depletion with unusual enrichments in REE evident by geochemical features of the carbonatites (e.g.[8]). Available data suggest that the melting of carbonate-rich siliciclastic sediments forms melt of granitic composition at lower pressures (2.5 GPa), and of phonolitic composition at higher pressures (5.0 GPa)[7]. Only at a higher temperature (> 1100 °C), the conjugate carbonatitic melt will combine with alkaline granitic to phonolitic melts. To date, however, systematic studies of the interaction between mantle and fluid/melt derived from the melting and dehydration of the mixed carbonate and silicate sediments are still lacking and our understanding of the underlying mechanism of this interaction remains limited.

In this study, we performed a series of 2 GPa sediment-peridotite reaction experiments in a piston-cylinder apparatus at 800 and 850 °C by combining carbonaceous pelites with either harzburgite or lherzolite in the presence of water (20 wt.% of the sediment). These experiments simulate the crust-mantle interactions and formation of mantle metasomes under fore-arc mantle conditions where pressures <3 GPa and temperatures <1000 °C prevail, and where expected strong dehydration of serpentinized peridotites below oceanic crust trigger flux melting/dissolution of overlying carbonaceous pelites. The metasomes produced in this study consist of clinopyroxene + phlogopite ± amphibole ± carbonate minerals that would be able to produce Si-undersaturated ultrapotassic melts (leucitites and kamafugites) during the further stages of orogenesis resulting in the reactivation of the accreted fore-arc mantle.

Fore-arc mantle as a metasome stowage

In orogens like the Alpine-Himalayan belt, a significant portion of Tertiary volcanic associations is characterized by universal enrichment of potassium coupled with invariably high incompatible trace element contents and an isotopic signature that compositionally overlaps the upper continental crust[3,9,10]. This has for a long time been a puzzling issue, especially for the mantle-derived lamproites (Si-saturated), and leucitites and kamafugites (Si-undersaturated), which have the most extreme compositions: K_2O up to 12 wt.%, $^{87}Sr/^{86}Sr$ up to 0.723, εNd down to -13 as well as highly forsteritic olivine (Fo up to 93 %) with $\delta^{18}O_{V\text{-}SMOW}$ values up to +11.5 ‰[2,3]. These data establish a connection between the volcanism and the massive crustal recycling that must have played a crucial role in the mantle source preconditioning of AHOB[10], and represent a global feature[11–13]. Some of the best-documented case studies come from AHOB, including the Upper Cretaceous Pontide and South Aegean arcs, but also Indonesian Batu Tara, Trans Mexican Volcanic Belt, Central and Southern Vosges Mts. of northeastern France within the European Variscan Belt etc.[9,14–18]. However, it is still enigmatic which segment of the arc architecture might constitute this enrichment and what physical and chemical mechanisms might underlie it. Nevertheless, a few scenarios concerning the physical mechanism of the fore-arc mantle preconditioning have been in previous literature. The involvement of small continental slivers that are characteristic of accretionary orogens such as those produced by the Cenozoic closure of the Tethys Ocean in the Alpine–Himalaya belt or modern-day Indonesia is of profound significance for this recycling[9,10,17,19]. In contrast to the steady-state subduction zone, their presence will ultimately provide isotopically old crustal material reappearing also later in post-orogenic lavas[2]. An alternative mechanism to arrive at a similar result is the stacking of mixed "cold plumes" under the orogenic wedge, composed of similar tectonic mélanges but derived from deeper within the subduction channels[20–22]. This model proposes that subducted sediments may move across the Benioff zone due to "delamination" and rise into the overlying mantle wedge[22] especially when they are carbonate-rich[23]. These plumes can transport the fertile subducted crustal materials towards hotter zones of the mantle wedge above the subducting plate.

Table 1. Starting materials, water source, capsule architecture, and conditions for the peridotite-crust reaction experiments. AVX: Harzburgite, KLB: Lherzolite, SD48: carbonaceous pelite.

#		% Water	Water Source	Mantle/ Crust	Capsule Design	Mantle	Crust	Duration Days	T °C	P GPa
E10	Reaction	20	H_2O	1/3	Modular	AVX & KLB	SD48	14	850	2
E15	Reaction	20	H_2O	1/3	Modular	AVX & KLB	SD48	14	800	2
E17	Reaction	20	$Mg(OH)_2$	3/5	Simple	AVX	SD48	13	800	2
E25	Reaction	20	$Mg(OH)_2$	3/5	Simple	KLB	SD48	13	800	2
E33	Reaction	20	$Mg(OH)_2$	3/5	Simple	AVX	SD48	13	850	2
E41	Reaction	20	$Mg(OH)_2$	3/5	Simple	KLB	SD48	14	850	2
E45A	Melting	20	H_2O		Simple		SD48	6	850	2
E45B	Melting	20	H_2O		Simple		SD48	7	800	2

Despite the challenge to provide the exact mechanism of fore-arc preconditioning, existing thermal, geophysical and geochemical models suggest that the area between fore-arc serpentinites and the source region of arc magmas may represent a more efficient ground for sediment recycling than previously assumed[24,25]. Subduction zone seismicity data coupled with new high P-T experiments suggest that in the fore-arc region increased fluid pressures produced by the melting of sediments will promote the occurrence of small magnitude earthquakes and episodic tremor and slip[26,27]. In this region, the melting of the subducted sedimentary material will take place well below 1000°C, and will be additionally forced by the fluids expelled from the underlying serpentinites[28]. Recent data on the subduction zone slab top temperatures as well as empirically obtained thermal models show that in many subduction zones hydrous sediments will begin to melt already in the fore-arc region[25,29]. Sediment melting will produce melts of different compositions, depending on the ratio between carbonate and silicate components. In each case, it is expected that the melt will not be able to induce melting of the overlying mantle, but will infiltrate and react with peridotite and metasomatize it, producing domains enriched in hydrous minerals[9,10,18].

Results

We conducted 6 sediment-peridotite reaction experiments at 800 and 850 °C and 2 GPa with carbonaceous sediments and either synthetic lherzolite or harzburgite, in which a layer of sediment was placed in the bottom of the noble metal capsule above the layer of diamond melt-trap (more details on starting compositions and two types of capsule architecture see in Supplementary Data File I). The experimental capsules were geochemically and mineralogically thoroughly characterized in Supplementary

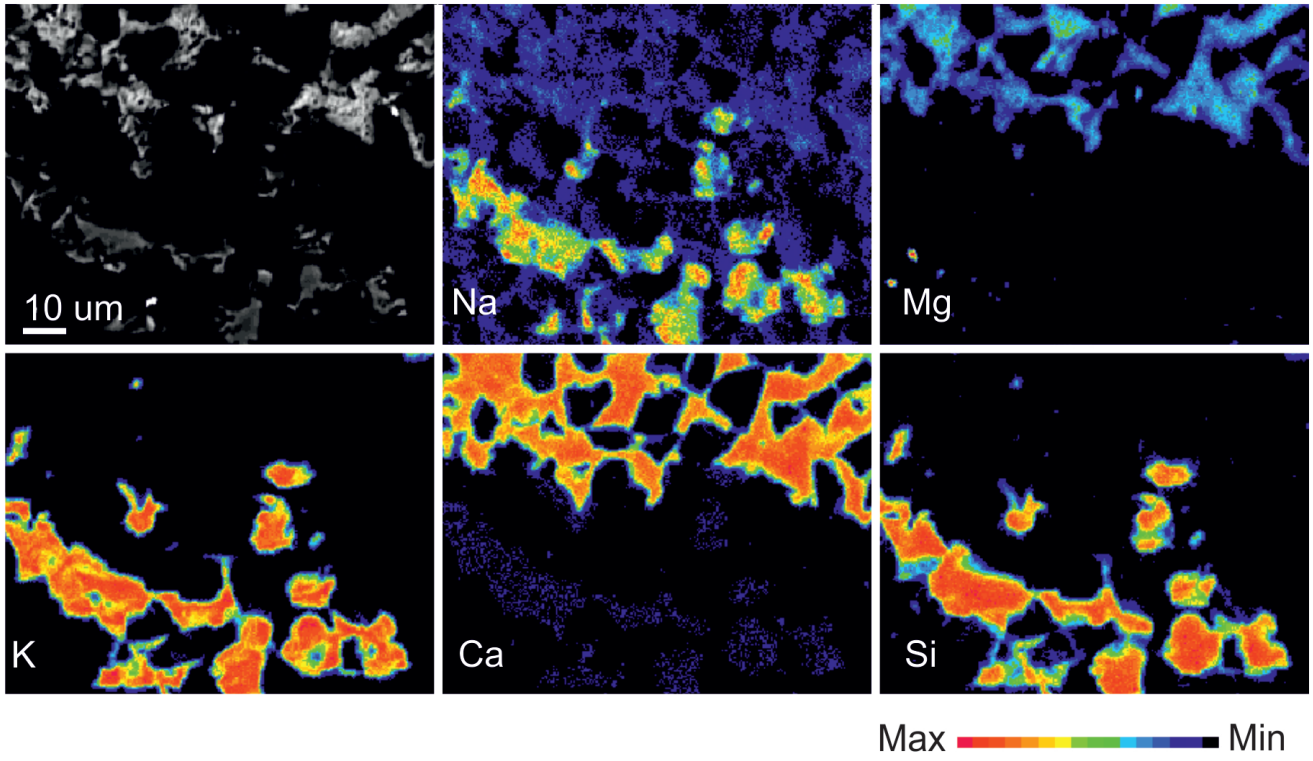

Figure 1. Element mapping reveals the composition of melts extracted due to the wet sediment melting during the reaction experiment at 800°C/2 GPa (Experiment 15B).

Data File I and comprehensive data set including major and trace elements of all experimental runs and melt compositions are presented in Supplementary Data File II.

Melt composition

In all experiments, two melt compositions were obtained in the melt trap: carbonate-rich and silica-rich, which we interpret as conjugate immiscible carbonatitic and silicic melts. It is important to mention that, at fore-arc depths low solute concentration fluids are referred to as aqueous fluids whereas high silicate concentration (> 65 wt.%) is adopted to be the marker of the melts[30]. Despite the significant controversies over the conditions controlling the formation and composition of the two liquids, aqueous fluids and melts are found to coexist at shallow depths of the mantle wedge at 2 GPa, 748 – 926 °C[30,31]. Given the compositional criteria and the conditions, that the hydrous silicic melts and aqueous fluids could coexist in our experiments, we prefer to define produced liquids as the hydrous carbonate and silicate melts, instead of deepening the argument over the melt and fluids in the mantle[32].

The experiment performed at 800°C/2 GPa (E15B), revealed that the conjugate melts are stratified (Figure 1), what was previously suggested to have resulted from density differences between compositionally contrasting melts[33]. In most cases, they are found to be either mingled or segregated within the voids of diamond grains to various extents (Figure 1). This relationship is a reminiscence of carbonate droplets separated from silicate glass along the veins of olivines observed in metasomatized mantle lherzolites as previously reported[34]. Besides two immiscible melts observed in the diamond trap, we have also found the carbonatitic melt in the peridotite part of the capsules regardless from the peridotite composition (Figure 2b and d).

The carbonatitic melts have totals as low as 50 wt.% and elevated CaO (13.5 – 48.3 wt.%), MgO (0.6 – 36.5 wt.%) and FeO(tot) (0.7 – 4.5 wt.%) with low NaO_2 and K_2O (av. 0.4 wt.% and 0.08 wt.%). There is a substantial difference in the carbonatitic melt composition within the trap and within the peridotite, with the latter having dolomitic Ca/(Ca + Mg) ratios of 0.38 – 0.60 (Figure 3a). The conjugate silicic melts are high in SiO_2(53.3 – 84.5 wt.%), Al_2O_3 (10.9 – 20.3 wt.%), and have extreme K_2O contents av. 9 wt.% (1.1 – 12.7 wt.%) (Figure 3b-c). Most of the silicic melt compositions are characterized by lower totals than 100 wt.% due to the high volatile contents. Analyses with totals below 80 wt.% were rejected.

In parallel two conjugate melts display characteristic carbonatite and silicate melt trace element variations; the silicate melt being enriched in LILE including Th and U, as well as Ti, Nb, Ta and Zr compared to the carbonatitic melt which is enriched in REE, Sr and P (Figure 6a). These variations can be better seen in particular ratios of trace element pairs such as Rb/Nb and

Th/La that are up to 5-fold higher in the silicic melts compared to the carbonatitic melts (Figure 6b).

Melt-peridotite interaction and formation of metasomes

There is no systematic difference between the lherzolitic and harzburgitic portions of the experimental charges in terms of the metasomatic mineral association resulting from the melt-peridotite interaction in our experiments: wehrlitization of peridotite with the replacement of Opx by Cpx represents the universal process, which is most intense in the nearest area closest to the sediment-peridotite interface (Figure 2a, c). However, all these interactions may appear as distinguished compositional variations in the same metasomatic or newly formed mineral species in the lherzolite- and harzburgite-sediment experiments. Opx and Cpx grains demonstrate significant disequilibrium textures, especially in the proximity of the sediment-peridotite interface, in contrast to spinel and olivine which are the least affected phases displaying no distinguishable textural changes (Figure 2b). Cpx is the most abundant newly formed and metasomatic phase in the reaction experiments. According to its relation with orthopyroxene, it can be grouped as follows:

- A rim of newly formed Cpx (Cpx-r, Figure 2a) surrounds Opx grains, partially resorb and detach them from the peridotite portion. Moreover, this type of Cpx occurs in the Cpx-Phl-Amph veins and pockets (Figure 2b-d). In lherzolite-sediment experiments, it is generally diopsidic (Mg# = 0.88–0.89; $Wo_{45-49}En_{45-48}$ Fs_6) with extreme enrichment in CaO up to 23.8 (wt.%) and has low contents of MgO (14.5 -16.9 wt.%) and Na_2O (0.1 - 0.2 wt.%) (Figure 5a-b). However, the Cr_2O_3 contents in Cpx from the reaction pockets are higher (0.46-0.51 wt.%) than in the Cpx from the interface (0.16 – 0.21 wt.%). On the contrary, in harzburgite - sediment reaction experiments reaction pocket Cpx are augite (Mg#= 0.91 – 0.92; Wo_{36-41} En_{54-58} Fs_{44-6}) with high Cr_2O_3 contents (2.0 – 2.7 wt.%) whereas Cpx from the interface display variation between augite and diopside with lower Cr_2O_3 contents (0.04 – 1.5 wt.%).
- Metasomatic Cpx (Cpx-m, dark colour, homogenous, euhedral crystals up to 20 μm) grains embay opx grains due to the melt invasion, dissolution and recrystallization processes (Figure 2b, c). The Cpx-m grains in lherzolite-sediment experiments are augitic and similar to Cpx from the unreacted peridotite portions (Mg#= 89–90; Wo_{35-39} En_{55-58} Fs_{6-7}, CaO 15.8- 17.7 wt.%, Na_2O 0.8 – 1.1 wt.%, Cr_2O_3 0.2 – 0.4 wt.%; Figure 2 a-b and 5a-b). The same type of Cpx in harzburgite-sediment experiments is similar (Mg#= 0.91 – 0.93; $Wo_{27-36}En_{58-66}$ Fs_{5-7}, CaO 14.2- 16.1 wt.%), but show slightly elevated MgO contents up to 24.1 wt.% (Figure5c). They also display variation in Cr_2O_3 (0.4 – 2.6 wt.%) and Na_2O (0.02 – 2.14 wt.%) (Figure 5d).

In addition to the newly formed Cpx (Cpx-r), phlogopite and amphibole are found as veins and domains together with dolomitic melt pockets within the peridotite (Figure 2b and 4). Phlogopite forms small bladed and/or acicular crystals (largest 7 x 0.2 μm) (Figure 2b). They are generally low in Ti (TiO_2< 0.8 wt.%) and in Cr (Cr_2O_3: 0.03 – 0.5 wt.%) and their Mg# is in the range between 85 and 92. The phlogopite crystals belonging to lherzolite-sediment reaction experiments (E10 and E15) display K_2O contents up to 7.8 wt.% and Cr_2O_3 between 0.4 – 0.5 wt.% with Mg# ranging 90 - 93. In contrast, phlogopites from harzburgite-sediment reaction experiments (E10 and E17) have broader variation in Mg# (85 - 93) and more elevated contents of K_2O (8.3 - 9.9 wt.%) with lower contents of Cr_2O_3 (0.03 – 0.15 wt.%) (Supplementary File I - Figure 1). Amphibole in lherzolite-sediment reaction experiments is pargasitic with high Mg#= 91. The composition of the accompanied carbonate minerals was not identified but elementary maps reveal their high Ca and low Si contents (Figure 4).
In summary, there is no systematic difference in the mineral assemblages forming metasomes within peridotite of different extents of depletion, and only their mineral composition reflects the more enriched (higher Ca, Al and Ti) character of the lherzolitic vs. harzburgitic host.

Discussion

New constraints on the petrogenesis of AHOB UP lavas

AHOB volcanic associations are generally characterized by universal enrichment of potassium coupled with invariably high incompatible trace element contents and isotopic compositions approaching crustal values (e.g[37] and references therein). In more detail, two compositionally different ultrapotassic volcanic series are recognized including Si-saturated leucite-free (lamproitic, shoshonitic and high-K calk-alkaline) series, and Si-undersaturated leucite-bearing series with kamafugites as the most primitive lavas[38–41]. Experimental data suggest that the primary melts of Si-saturated series require high-degree melting of a phlogopite-bearing mantle source[2,42–49]. On the other hand, ultrapotassic Si-undersaturated primary melts will be sourced in the peridotite fluxed by the volatile components H_2O and CO_2, or alternatively in the wehrlitic mantle with the presence of metasomatic phases such as dolomite, phlogopite and amphibole[50–54]. A single experimental study investigated the interaction between limestone and peridotite at upper mantle conditions, ultimately producing alkaline reaction melts[23].
Our experiments demonstrate that wehrlitisation is universally caused by sediment-melt interaction with peridotite due to carbonatite metasomatism, as previously observed (e.g.,[55–58]). Moreover, the immiscible carbonatitic and silicic melts which

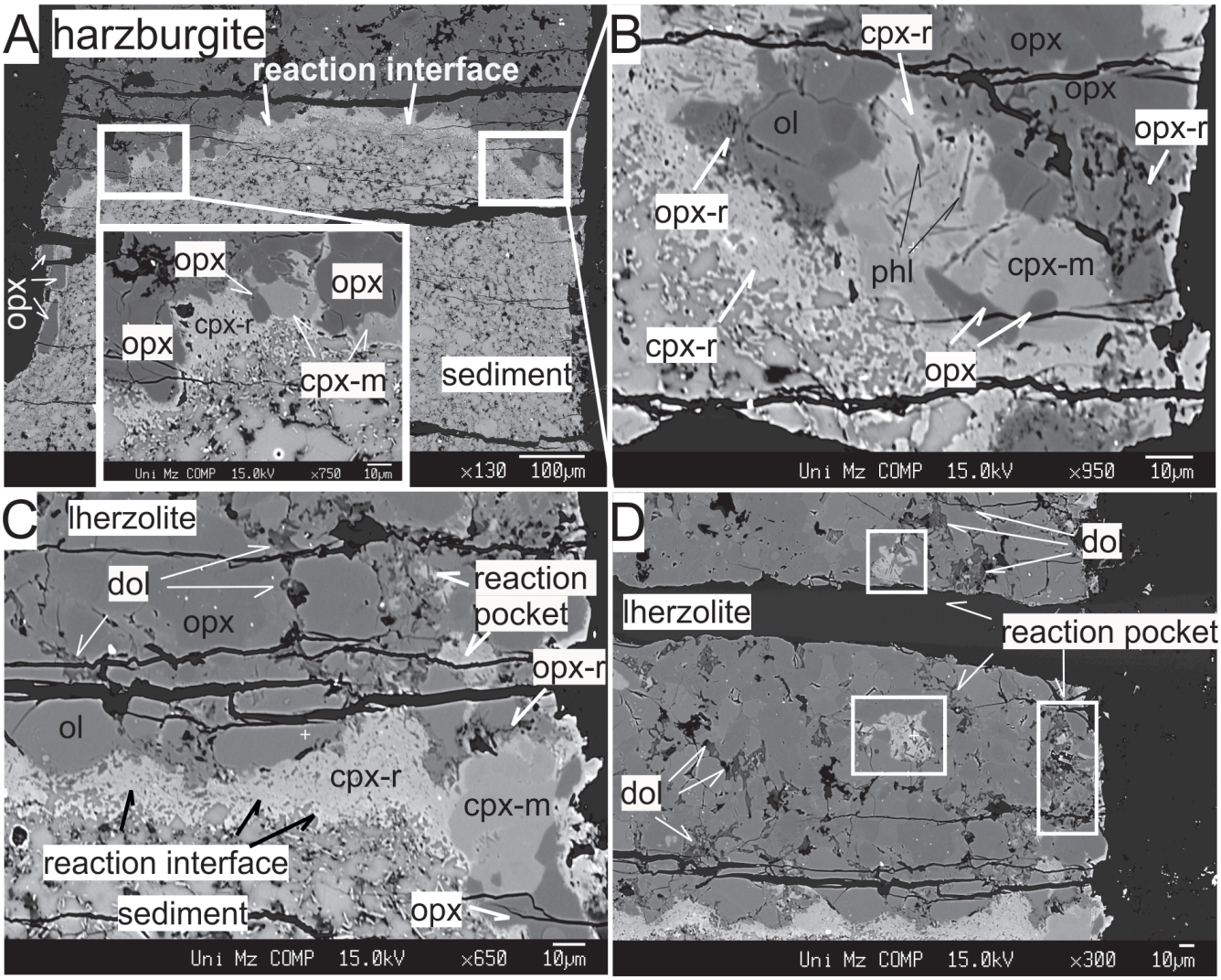

Figure 2. Backscattered electron images of the experimental charges revealing the formation of metasomatic minerals due to reaction of sediment with peridotite. a) The reaction interface seen as a bright film layer between mantle and crust in harzburgite-sediment reaction experiment at 850 ^{o}C/2 GPa, b) Closer view revealing the embayment of Opx by metasomatic Cpx (Cpx-m), the development of sieve texture in newly formed Opx(Opx-r) and of inclusions of phlogopite needles in Cpx (Cpx-r); olivine (ol) remained intact, c) The reaction interface dominated by the second generation clinopyroxenes and poorly developed reaction pockets seen at right top corner (lherzolite-sediment reaction experiment at 850 ^{o}C/2 GPa), d) Dolomitic melt ponds and reaction pockets (ol: olivine, opx: orthopyroxene, opx-r: second generation orthopyroxene, cpx-m: metasomatic clinopyroxene, cpx-r: second generation clinopyroxene, phl: phlogopite, cb: carbonate minerals, amp: amphibole, dol: dolomitic glass)

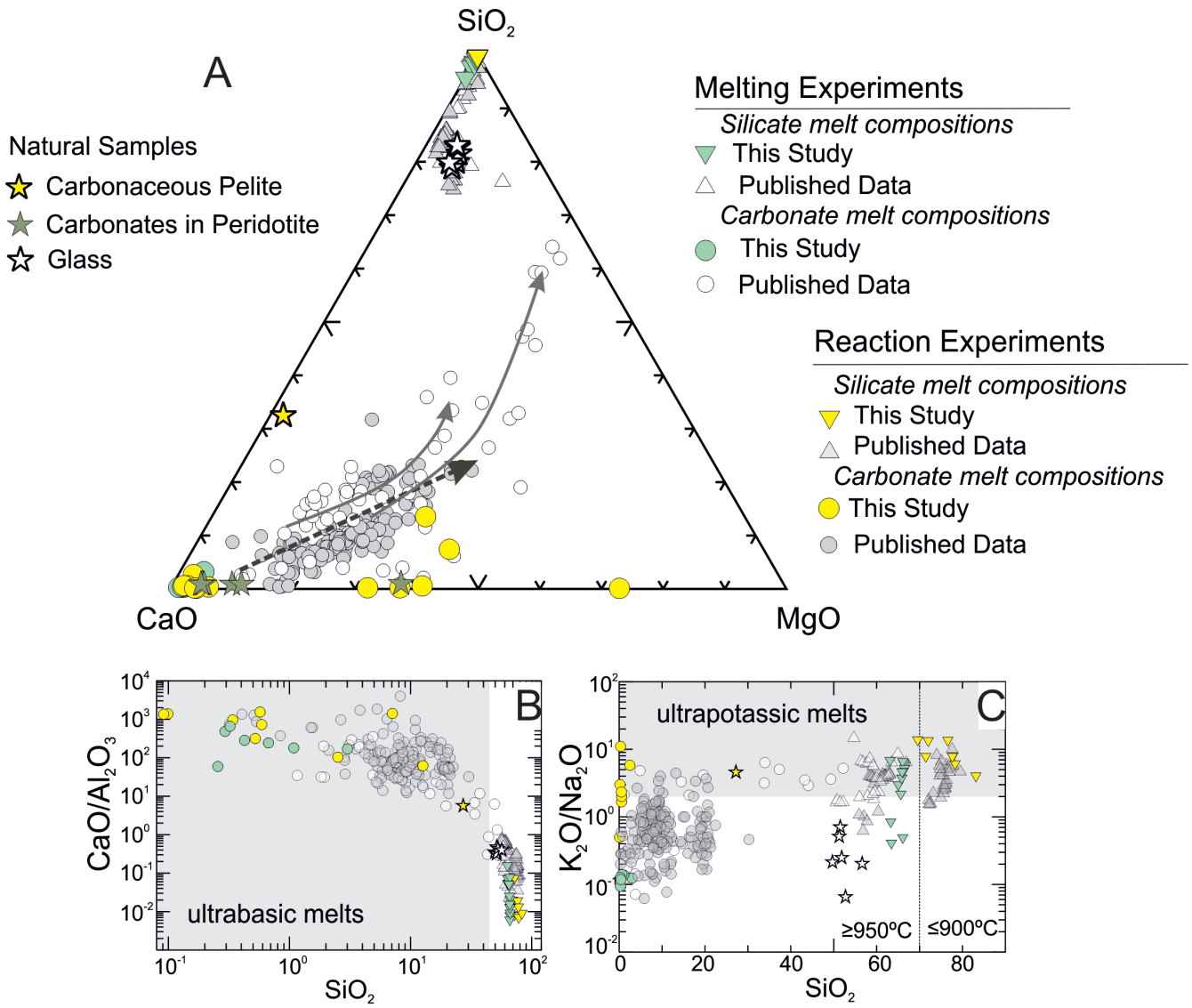

Figure 3. The chemical compositions of the hydrous carbonate and silicate melts in this study in comparison with previous experimental products and with melts detected in natural peridotite samples. The arrows indicating the evolutionary trends of melt compositions with increasing temperature are taken from other experimental studies[23,35,36].

released from the carbonaceous pelite interact with peridotites to form low-density assemblages of several hydrous minerals and dolomite within werhlite. The mineral assemblage produced, that is, a wehrlitic peridotite with phlogopite, amphibole and carbonate minerals (Figure 4) perfectly matches the proposed mantle source compositions of the orogenic Si-undersaturated ultrapotassic magmatism accounting for the K-enrichment and silica depletions.

The phlogopites are characterized by low Ti and Cr contents, comparable with those in similar reaction experiments and natural xenolith samples[46,59] (Supplementary Data File I- Figure 7). The composition of the carbonate minerals in the metasomes has been inferred to be dolomite-type based on the elementary maps revealing that Ca and Mg are proportionally equal in these occurrences (Figure 4). This is partly comparable with the mantle wedge peridotites which host Mg-Calcite and dolomite[34,60]. The presence of phlogopite and carbonate minerals is accepted as sole evidence of modal metasomatism[59,61,62] and various metasomatic agents in a range of composition and conditions are held responsible for their generation[63,64].

For example, the Mount Leura xenoliths from Victoria State, Australia were suggested to indicate the leading of K-Na-OH-rich fluids in a peridotite ambient under reduced conditions based on the thermodynamic modelling of the system[59]. Moreover, these fluids and melts are also suggested to might have originated from various media (subducted slab, convective asthenosphere and uprising plume[70]. This variety in proposed mantle sources of the metasomatic agents is not unexpected because identification of the metasomatic components percolating the upper mantle is challenging: they can not be examined directly, but can be

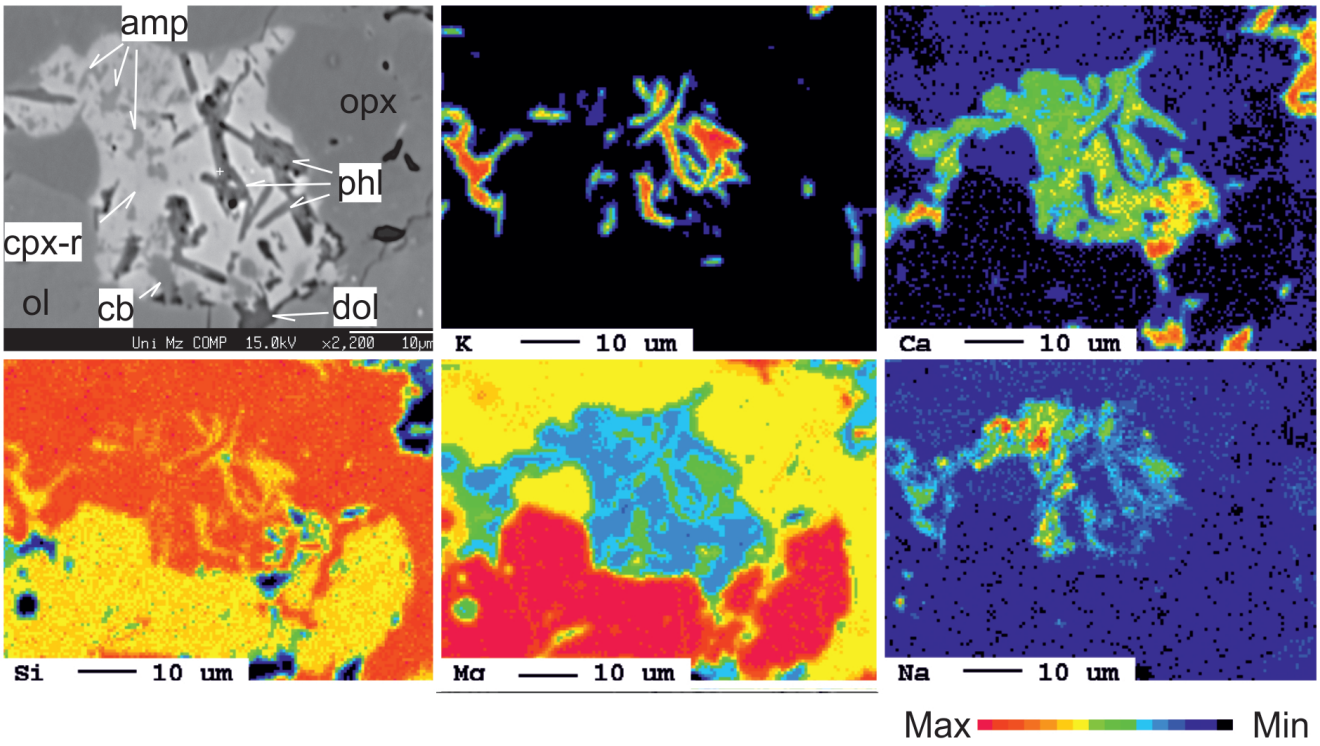

Figure 4. Element mapping revealing the mineral paragenesis of the metasome that formed by the reaction of carbonaceous pelite and lherzolite (E-10) at 850 °C/2 GPa (see Figure 2 caption for the abbreviations).

inferred from fluid and solid inclusions in primary minerals of deep xenoliths, peridotite massifs and eclogites, and modelling based on trace element compositions of alkali basalts, carbonatites and/or mantle minerals. In this respect, the finding of the immiscible and conjugate melts in our experiments is of greate importance, therefore we can especially ascribe specific element enrichments to the different melt compositions.

In summary, our experiments demonstrate that phlogopite, pargasite and carbonate minerals can grow within the mantle wedge as a consequence of slab-fore-arc interaction, resulting in metasomatic domains within the depleted peridotite mantle. Its later activation will preferentially involve these domains which are internally heterogeneous on scales similar to those of melting and magma extraction (i.e. metres to kilometres), as suggested by isotopic data[10], to form silica-undersaturated ultrapotassic melts if the degree of partial melting is not too low[71,72]. We favour a combination of the mélange diapir model which provides a minimalistic approach and the conventional model which requires a combination of dehydration, melting and mixing processes of various components.

The Th/La conundrum revisited

Besides potassium, trace element and isotopic enrichments, the Si-saturated AHOB lavas (lamproites) demonstrate a positive correlation of extremely high Th/La with the high Sm/La[19] whereas it is absent in Si-undersaturated lavas. This kind of enrichment is inconsistent with a mantle source metasomatized by slab-derived components including recycling of the subducted sediments because Sm/La doesn't show a positive correlation with the Th/La ratio in arc magmas that is also never greater than 0.5[73] (Figure 6). Moreover, it is not observed in the crust, the mantle, or in mantle-derived melts generally, suggesting that either some unusual source or previously unrevealed process may be responsible for this enrichment. The most recent and comprehensive treatment of the subject has been given by researchers[19] who have also reviewed the most important solutions to this conundrum. These include the presence of a fictional ancient component (coined SALATHO) enriched in lawsonite that can considerably fractionate Th and La and provide high Th/La and Sm/La, which possibly has been stored in the recycled mélange in form of diapir within the mantle[74–76]. An important aspect not fully addressed[19], is the extent to which several other ingredients, including high K and the extreme isotopic signature, are provided in the mélange to satisfy the compositional enrichment observed in AHOB ultrapotassic lavas.

Our experiments support an alternative explanation for this paradox. Conjugate carbonatitic and silicic melts generated by melting of the carbonaceous pelites demonstrate substantial differences in trace element concentrations and ratios (Figure 6a-b). If we focus on the Th/La ratios in the hydrous and K-rich silicic melt, it is up to 5-fold higher than in the carbonatitic

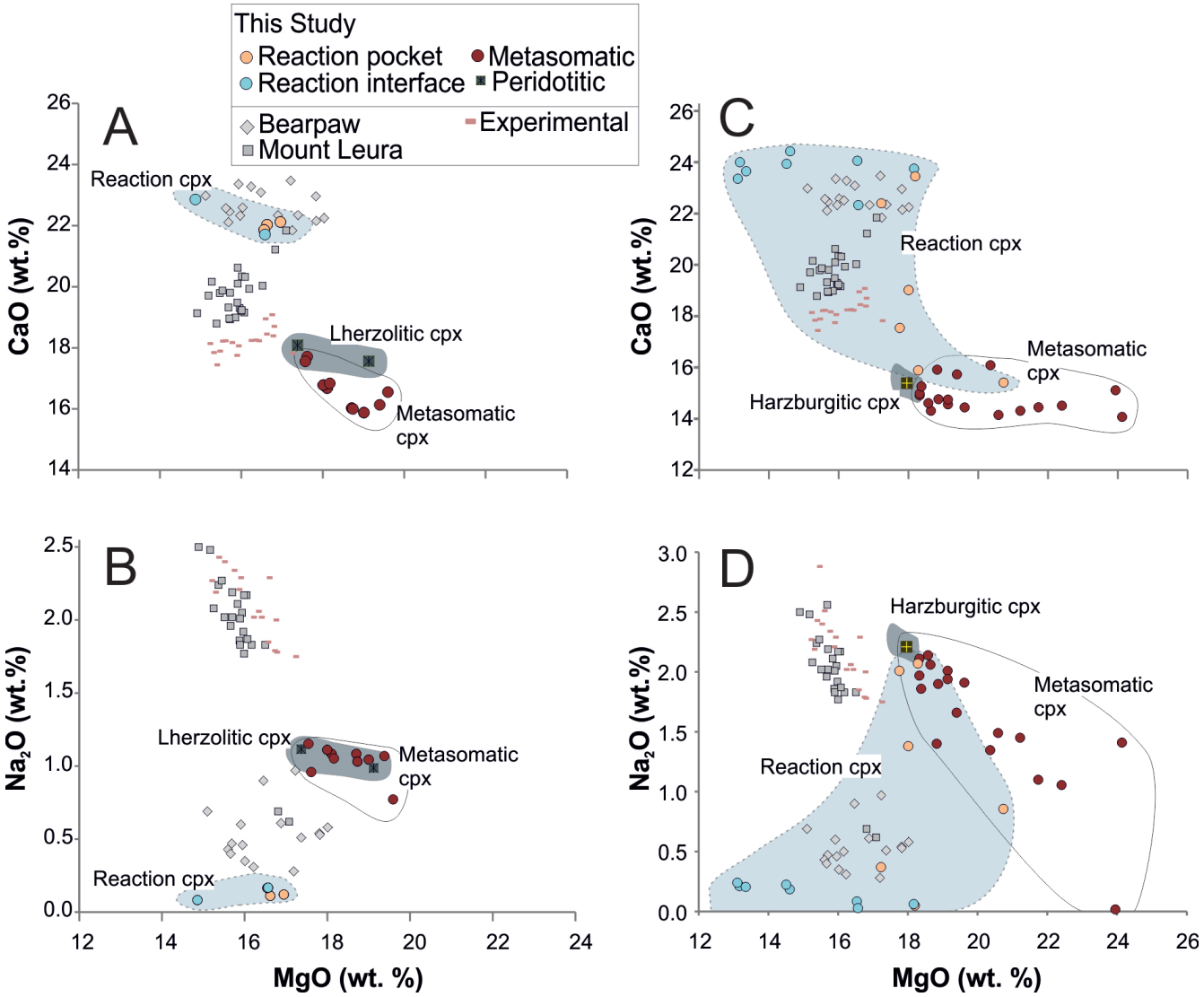

Figure 5. MgO (wt.%) vs. Na_2O and CaO (wt.%) variation diagrams for the clinopyroxene subgroups in lherzolite-marl (a-b) and harzburgite-marl (c-d) reaction experiments. For comparison, clinoproxene measuments from the synthetic lherzolite and harzburgite prepared for this study are plotted. The clinopyroxene data from other reaction experiments[46], as well as natural xenoliths of Bearpaw[65] and Mount Leura[59] are plotted.

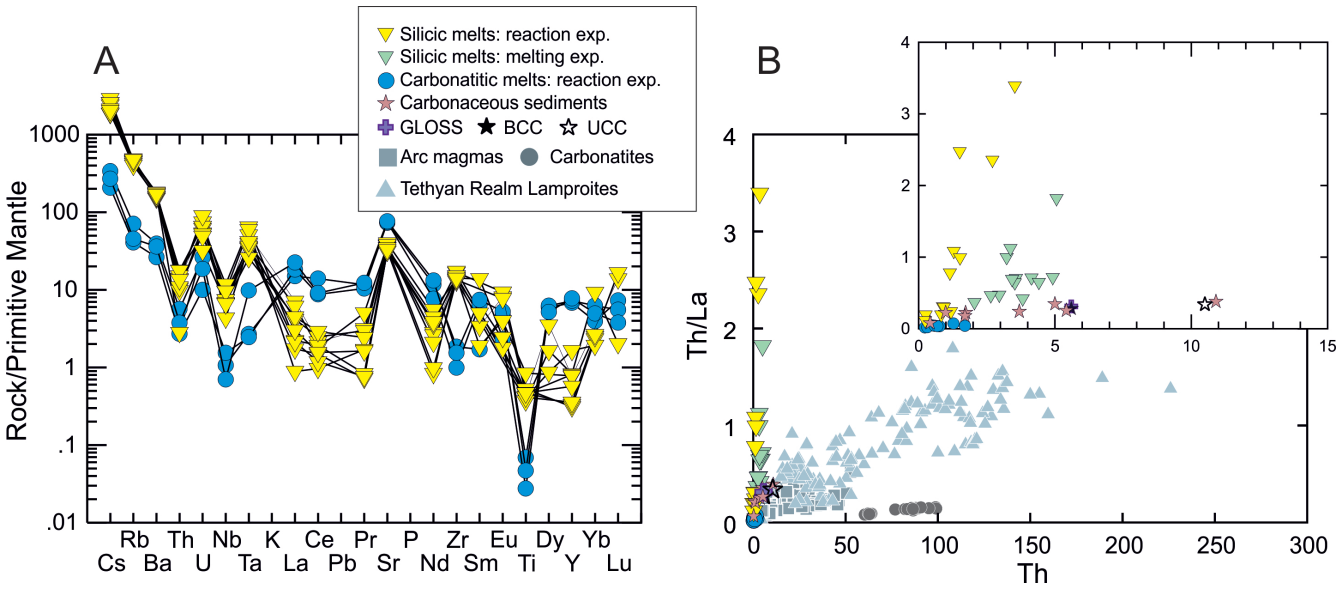

Figure 6. a) Primitive mantle normalized trace element patterns of the representative conjugate carbonatitic and silicic melts from sediment-peridotite reaction experiments. Primitive mantle value is from[66]. b) Th vs. Th/La diagram for the carbonatitic melts from reaction experiments with silicate melts from reaction and melting experiments in this study. Carbonaceous sediments[37], global subducting sediment (GLOSS[67]), bulk continental crust (BCC[68]), upper continental crust (UCC[68]), arc magmas (Pontide arc ultrapotassic rocks[9]), carbonatites (Mt. Vulture Carbonatites[69]), Tethyan Realm Lamproites[19] are also plotted for comparison.

melt, due to the very intense fractionation of these two elements (Figure 6b). This kind of fractionation is in accordance with experimentally determined carbonatite/silicate melt partition coefficients obtained in the hydrous K-rich silicic systems[77]. We assume that this geochemical fingerprint will be effectively conveyed to the silicate portion of the mantle, mostly in the phlogopite-clinopyroxene-rich metasomes. It will be provided by silicate melt separated from the conjugate carbonatitic melt, which will have all ingredients proposed to build a metasomatized source of lamproites: extreme potassium enrichment, variable but high Sm/La ratio, extremely high Th/La ratios, as well as extremely radiogenic isotopic signatures. In other words, if the metasomes are generated by the recycling of carbonate-rich sediments within the mantle wedge, their melting will produce the magmas with the same fingerprint. We envisage that during subduction-induced sediment recycling and cyclic metasomatism that is active at the slab-(fore-arc) mantle interface, the dense alkaline fluids will migrate upward by means of cycles of melting, solidifying/freezing and reacting as subduction progresses[24,78]. We speculate that the melting of the carbonaceous sediments will successfully yield an alkaline dolomitic melt and a hydrous silicate and potassic melt. The infiltration of these distinct melts into depleted mantle may result in decoupled metasomatic events. First, metasomatism by the dolomitic melt creates a trend from harzburgite to olivine-rich wehrlite. If the melting will take place in the metasomatized region comprising of the dolomite-bearing phlogopite wehrlites, the melting of the metasomes will produce kamafugite that by default doesn't show a Th/La anomaly. As the melt transmission through the peridotite involves multistage processes, we envisage that its interaction with the peridotitic mantle will result in silica and potassium enrichment and depletion in HFSEs relative to LILE situated within the universally present phlogopite clinopyroxenites[46,79]. In the case the two melts have been separated within the mantle due to differences in viscosity and permeability, the infiltration of the silicate melt enriches the metasomatized rocks in clinopyroxene and phlogopite, which after melting will produce lamproites showing the Th/La anomaly. These multiple imprints of the recycled sedimentary materials in the relatively restricted area have been described in the Italian arc, in Latera volcano[80] as well as in San Venanzo[3], where both Si-saturated (lamproitic) and Si-undersaturated (leucititic and kamafugitic) melts and derivative minerals have been observed. This is also in accordance with the recent studies investigating the fate of the CO_2 in the upper mantle, underscoring that the Tethyan subduction might have transported a much larger amount of CO_2 than previously assumed[71,76,81]. Moreover, it is also recently proposed that the recycled carbonate sediments are responsible for low δ^{26}Mg and high δ^{66}Zn signatures observed in the Mediterranean lamproites defining so-called "Mg-Zn isotopic decoupling"[82].

Conclusion

We can draw following conclusions from our study:

- In a series of 2 GPa experiments in a piston-cylinder apparatus at 800 and 850 ^{o}C, we combine carbonaceous pelites

with either harzburgite or lherzolite in the presence of water (20 wt.% of the sediment), simulating the crust-mantle interactions and formation of mantle metasomes in fore-arc mantle conditions.

- Two conjugate melts, that is, carbonatitic and ultra-high-K silicate melts are produced, representing strong metasomatizing agents.
- The metasomes produced consist of clinopyroxene + phlogopite ± amphibole ± carbonate minerals that would be able to produce Si-undersaturated ultrapotassic melts (leucitites and kamafugites) during the further stages of orogenesis resulting in the post-collisional reactivation of the accreted fore-arc mantle.
- Two conjugate melts demonstrate a strong potential for incompatible trace-element fractionation, with silicate portions driving high Th/La, Sm/Nd and LILE/HFSE, as being observed in Si-saturated utrapotassic lavas.

Methods

Selection of Starting Materials and Capsule Design

Starting materials were composed of the synthetic mantle and natural lithologies. To prepare the peridotite end-members, high-purity, commercially available oxide powders (SiO_2, TiO_2, Al_2O_3, Fe_2O_3, K_2O, Na_2O, MgO, CaO, Cr_2O_3, NiO and MnO) were mixed with ethanol in an agate mortar and pestle for more than 2h and were synthesized at 1250 ^oC/2 GPa according to the standart procedure by Rapp et al. (1999). Fertile peridotite is a natural spinel lherzolite sample (KLB-1) from Kilbourne Hole, USA[83], while the depleted peridotite (AVX) is a harzburgite from Volvoyam Volcanic Field, Kamchatka Arc[84].

The natural sediment sample is a carbonaceous pelite - marlstone from the Apennine Region (SD48), which is geochemically characterized by Avanzinelli et al (2008) and Conticelli et al. (2009) and discussed as one of the potential end members involved in crustal recycling within the mantle source of Italian ultrapotassic magmatism. The reaction experiments were performed in two different types of capsule designs. The further details of the capsules and the compositions of the starting materials are given in Supplementary File I.

Experimental Procedure

The experiments in this study have been conducted using the piston cylinder apparatus in the Experimental Petrology Laboratory at Johannes Gutenberg University Mainz (JGU) . The reaction experiments were performed at 800 - 850 ^oC and 2 GPa. The first two runs were performed with modular capsules at 850 ^oC and 800 ^oC/2 GPa and the following runs with simple design repeated under the same conditions separately for the combinations of the harzburgite + marl and the lherzolite + marl (Table 1). Melting experiments (6 days) have been conducted under the same conditions as reaction experiments (15 days) but for a shorter duration.

Analytical Methods

The polished experimental charges were imaged and the mineral and melt phases were analyzed using the JEOL JXA 8200 Superprobe at JGU for electron probe microanalyzation (EPMA). Operating conditions were set to 20 kV accelerating voltage, 20 nA beam current and 2 nm beam diameter. Synthetic and natural minerals were used as reference materials. To better document reactions between mantle and crust under given conditions backscattered electron images of the reaction zones and metasomatic portions were produced. We identified the melt composition by measuring glasses which are devoid of quench crystals throughout the experimental charges. Where sufficiently large melt pockets are absent, element distribution maps were produced to document the glass compositions (Figure 1). The diamond trap drained the initial melts from the sediment and helped us with the accurate determination of unfractionated melt compositions.

Trace element analyses of the glasses were performed by LA-ICP-MS at the University of Mainz using an ArF EXCIMER-laser (193 nm wavelength, NWR193 system by esi/NewWave) coupled to an Agilent 7500ce ICP-MS system according to the standard procedure described in[9]. The measurements were calibrated based on the NIST 610, NIST 612 and BCR glass reference materials. Iron-loss from the system to the Au-Pd outer capsule was calculated and found to be insignificant based on mass balance (Supplementary File II). We also employed mass balance calculations to justify the visually estimated modal proportions of the mineral and melt phases.

References

1. Hole, M. Post-subduction alkaline volcanism along the antarctic peninsula. *J. Geol. Soc.* **145**, 985–998 (1988).
2. Prelević, D., Foley, S., Romer, R. & Conticelli, S. Mediterranean tertiary lamproites derived from multiple source components in postcollisional geodynamics. *Geochimica et Cosmochimica Acta* **72**, 2125–2156 (2008).

3. Günther, J. *et al.* Subduction-legacy and olivine monitoring for mantle-heterogeneities of the sources of ultrapotassic magmas: The italian case study. *Geochem. Geophys. Geosystems* e2022GC010709.
4. Kessel, R., Schmidt, M. W., Ulmer, P. & Pettke, T. Trace element signature of subduction-zone fluids, melts and supercritical liquids at 120–180 km depth. *Nature* **437**, 724–727 (2005).
5. Scambelluri, M. & Philippot, P. Deep fluids in subduction zones. *Lithos* **55**, 213–227 (2001).
6. Tatsumi, Y. & Kogiso, T. Trace element transport during dehydration processes in the subducted oceanic crust: 2. origin of chemical and physical characteristics in arc magmatism. *Earth Planet. Sci. Lett.* **148**, 207–221 (1997).
7. Thomsen, T. B. & Schmidt, M. W. Melting of carbonated pelites at 2.5–5.0 gpa, silicate–carbonatite liquid immiscibility, and potassium–carbon metasomatism of the mantle. *Earth Planet. Sci. Lett.* **267**, 17–31 (2008).
8. Hoernle, K., Tilton, G., Le Bas, M. J., Duggen, S. & Garbe-Schönberg, D. Geochemistry of oceanic carbonatites compared with continental carbonatites: mantle recycling of oceanic crustal carbonate. *Contributions to Mineral. Petrol.* **142**, 520–542 (2002).
9. Gülmez, F. *et al.* Ultrapotassic volcanism from the waning stage of the neotethyan subduction: a key study from the izmir–ankara–erzincan suture belt, central northern turkey. *J. Petrol.* **57**, 561–593 (2016).
10. Prelević, D., Jacob, D. E. & Foley, S. F. Recycling plus: a new recipe for the formation of alpine–himalayan orogenic mantle lithosphere. *Earth Planet. Sci. Lett.* **362**, 187–197 (2013).
11. Gao, Y. *et al.* Lamproitic rocks from a continental collision zone: evidence for recycling of subducted tethyan oceanic sediments in the mantle beneath southern tibet. *J. Petrol.* **48**, 729–752 (2007).
12. Hao, L.-L. *et al.* Contribution of continental subduction to very light b isotope signatures in post-collisional magmas: evidence from southern tibetan ultrapotassic rocks. *Earth Planet. Sci. Lett.* **584**, 117508 (2022).
13. Zhao, Z. *et al.* Geochemical and sr–nd–pb–o isotopic compositions of the post-collisional ultrapotassic magmatism in sw tibet: petrogenesis and implications for india intra-continental subduction beneath southern tibet. *Lithos* **113**, 190–212 (2009).
14. Hora, J. M., Tabaud, A.-S., Janoušek, V. & Kochergina, Y. V. E. Potassic magmas of the vosges mts.(ne france) delimit the areal extent and nature of long-gone variscan orogenic mantle domains. *Lithos* **402**, 106304 (2021).
15. Luhr, J. F., Allan, J. F., Carmichael, I. S., Nelson, S. A. & Hasenaka, T. Primitive calc-alkaline and alkaline rock types from the western mexican volcanic belt. *J. Geophys. Res. Solid Earth* **94**, 4515–4530 (1989).
16. Soder, C., Altherr, R. & Romer, R. L. Mantle metasomatism at the edge of a retreating subduction zone: Late neogene lamprophyres from the island of kos, greece. *J. Petrol.* **57**, 1705–1728 (2016).
17. Stolz, A., Varne, R., Wheller, G., Foden, J. & Abbott, M. The geochemistry and petrogenesis of k-rich alkaline volcanics from the batu tara volcano, eastern sunda arc. *Contributions to Mineral. Petrol.* **98**, 374–389 (1988).
18. Vigouroux, N., Wallace, P. J. & Kent, A. J. Volatiles in high-k magmas from the western trans-mexican volcanic belt: evidence for fluid fluxing and extreme enrichment of the mantle wedge by subduction processes. *J. Petrol.* **49**, 1589–1618 (2008).
19. Tommasini, S., Avanzinelli, R. & Conticelli, S. The th/la and sm/la conundrum of the tethyan realm lamproites. *Earth Planet. Sci. Lett.* **301**, 469–478 (2011).
20. Castro, A. & Gerya, T. Magmatic implications of mantle wedge plumes: Experimental study. *Lithos* **103**, 138–148 (2008).
21. Gerya, T. V. & Yuen, D. A. Rayleigh–taylor instabilities from hydration and melting propel 'cold plumes' at subduction zones. *Earth Planet. Sci. Lett.* **212**, 47–62 (2003).
22. Jull, M. & Kelemen, P. á. On the conditions for lower crustal convective instability. *J. Geophys. Res. Solid Earth* **106**, 6423–6446 (2001).
23. Chen, C., Förster, M. W., Foley, S. F. & Liu, Y. Massive carbon storage in convergent margins initiated by subduction of limestone. *Nat. communications* **12**, 1–9 (2021).
24. Förster, M. & Selway, K. Melting of subducted sediments reconciles geophysical images of subduction zones. *Nat. communications* **12**, 1–7 (2021).
25. Klein, B. Z. & Behn, M. D. On the evolution and fate of sediment diapirs in subduction zones. *Geochem. Geophys. Geosystems* **22**, e2021GC009873 (2021).
26. Obara, K. Nonvolcanic deep tremor associated with subduction in southwest japan. *Science* **296**, 1679–1681 (2002).

27. Rubinstein, J. L., Shelly, D. R. & Ellsworth, W. L. Non-volcanic tremor: A window into the roots of fault zones. *New Front. Integr. Solid Earth Sci.* 287–314 (2010).

28. Hermann, J. & Spandler, C. J. Sediment melts at sub-arc depths: an experimental study. *J. Petrol.* **49**, 717–740 (2008).

29. Syracuse, E. M., van Keken, P. E. & Abers, G. A. The global range of subduction zone thermal models. *Phys. Earth Planet. Interiors* **183**, 73–90 (2010).

30. Ni, H., Zhang, L., Xiong, X., Mao, Z. & Wang, J. Supercritical fluids at subduction zones: Evidence, formation condition, and physicochemical properties. *Earth-Science Rev.* **167**, 62–71 (2017).

31. Kawamoto, T., Kanzaki, M., Mibe, K., Matsukage, K. N. & Ono, S. Separation of supercritical slab-fluids to form aqueous fluid and melt components in subduction zone magmatism. *Proc. Natl. Acad. Sci.* **109**, 18695–18700 (2012).

32. Hermann, J., Zheng, Y.-F. & Rubatto, D. Deep fluids in subducted continental crust. *Elements* **9**, 281–287 (2013).

33. Brooker, R. & Hamilton, D. Three-liquid immiscibility and the origin of carbonatites. *Nature* **346**, 459–462 (1990).

34. Laurora, A. *et al.* Metasomatism and melting in carbonated peridotite xenoliths from the mantle wedge: the gobernador gregores case (southern patagonia). *J. Petrol.* **42**, 69–87 (2001).

35. Foley, S. *et al.* The composition of near-solidus melts of peridotite in the presence of co2 and h2o between 40 and 60ákbar. *Lithos* **112**, 274–283 (2009).

36. Weidendorfer, D., Manning, C. E. & Schmidt, M. W. Carbonate melts in the hydrous upper mantle. *Contributions to Mineral. Petrol.* **175**, 1–17 (2020).

37. Conticelli, S. *et al.* Trace elements and sr–nd–pb isotopes of k-rich, shoshonitic, and calc-alkaline magmatism of the western mediterranean region: genesis of ultrapotassic to calc-alkaline magmatic associations in a post-collisional geodynamic setting. *Lithos* **107**, 68–92 (2009).

38. Conticelli, S. *et al.* Leucite-bearing (kamafugitic/leucititic) and-free (lamproitic) ultrapotassic rocks and associated shoshonites from italy: constraints on petrogenesis and geodynamics. *J. Virtual Explor.* **36**, 1–95 (2010).

39. Conticelli, S., Avanzinelli, R., Ammannati, E. & Casalini, M. The role of carbon from recycled sediments in the origin of ultrapotassic igneous rocks in the central mediterranean. *Lithos* **232**, 174–196 (2015).

40. Foley, S., Venturelli, G., Green, D. & Toscani, L. The ultrapotassic rocks: characteristics, classification, and constraints for petrogenetic models. *Earth-Science Rev.* **24**, 81–134 (1987).

41. Peccerillo, A. & internationale de volcanologie et de chimie de l'intérieur de la Terre, A. *Cenozoic volcanism in the Tyrrhenian Sea region* (Springer, 2017).

42. Foley, S. Vein-plus-wall-rock melting mechanisms in the lithosphere and the origin of potassic alkaline magmas. *Lithos* **28**, 435–453 (1992).

43. Condamine, P. & Médard, E. Experimental melting of phlogopite-bearing mantle at 1 gpa: Implications for potassic magmatism. *Earth Planet. Sci. Lett.* **397**, 80–92 (2014).

44. Condamine, P., Médard, E. & Devidal, J.-L. Experimental melting of phlogopite-peridotite in the garnet stability field. *Contributions to Mineral. Petrol.* **171**, 1–26 (2016).

45. Förster, M. W. *et al.* Melting phlogopite-rich marid: Lamproites and the role of alkalis in olivine-liquid ni-partitioning. *Chem. Geol.* **476**, 429–440 (2018).

46. Förster, M. W., Prelević, D., Buhre, S., Mertz-Kraus, R. & Foley, S. F. An experimental study of the role of partial melts of sediments versus mantle melts in the sources of potassic magmatism. *J. Asian Earth Sci.* **177**, 76–88 (2019).

47. Mallik, A., Dasgupta, R., Tsuno, K. & Nelson, J. Effects of water, depth and temperature on partial melting of mantle-wedge fluxed by hydrous sediment-melt in subduction zones. *Geochimica et cosmochimica acta* **195**, 226–243 (2016).

48. Thibault, Y. & Edgar, A. Patent mantle-metasomatism: inferences based on experimental studies. *Proc. Indian Acad. Sci. Planet. Sci.* **99**, 21–37 (1990).

49. Wang, Y., Foley, S. F. & Prelević, D. Potassium-rich magmatism from a phlogopite-free source. *Geology* **45**, 467–470 (2017).

50. Naemura, K., Hirajima, T., Svojtka, M., Shimizu, I. & Iizuka, T. Fossilized melts in mantle wedge peridotites. *Sci. Reports* **8**, 1–12 (2018).

51. Olafsson, M. & Eggler, D. H. Phase relations of amphibole, amphibole-carbonate, and phlogopite-carbonate peridotite: petrologic constraints on the asthenosphere. *Earth Planet. Sci. Lett.* **64**, 305–315 (1983).

52. Wendlandt, R. F. & Eggler, D. H. The origins of potassic magmas; 2, stability of phlogopite in natural spinel lherzolite and in the system kalsio 4-mgo-sio 2-h 2 o-co 2 at high pressures and high temperatures. *Am. J. Sci.* **280**, 421–458 (1980).

53. Wyllie, P. J. Mantle fluid compositions buffered by carbonates in peridotite. *The J. Geol.* **85**, 187–207 (1977).

54. Wallace, M. E. & Green, D. H. An experimental determination of primary carbonatite magma composition. *Nature* **335**, 343–346 (1988).

55. Rudnick, R. L., McDonough, W. F. & Chappell, B. W. Carbonatite metasomatism in the northern tanzanian mantle: petrographic and geochemical characteristics. *Earth Planet. Sci. Lett.* **114**, 463–475 (1993).

56. Yaxley, G. M., Crawford, A. J. & Green, D. H. Evidence for carbonatite metasomatism in spinel peridotite xenoliths from western victoria, australia. *Earth Planet. Sci. Lett.* **107**, 305–317 (1991).

57. Yaxley, G. M., Green, D. H. & Kamenetsky, V. Carbonatite metasomatism in the southeastern australian lithosphere. *J. Petrol.* **39**, 1917–1930 (1998).

58. Zinngrebe, E. & Foley, S. Metasomatism in mantle xenoliths from gees, west eifel, germany: evidence for the genesis of calc-alkaline glasses and metasomatic ca-enrichment. *Contributions to Mineral. Petrol.* **122**, 79–96 (1995).

59. Bonadiman, C. *et al.* Phlogopite-pargasite coexistence in an oxygen reduced spinel-peridotite ambient. *Sci. Reports* **11**, 1–17 (2021).

60. Andersen, T. & Neumann, E.-R. Fluid inclusions in mantle xenoliths. *Lithos* **55**, 301–320 (2001).

61. Pearson, D., Canil, D. & Shirey, S. Mantle samples included in volcanic rocks: xenoliths and diamonds. *Treatise on geochemistry* **2**, 568 (2003).

62. Roden, M. F. & Murthy, V. R. Mantle metasomatism. *Annu. Rev. Earth Planet. Sci.* **13**, 269–296 (1985).

63. Foley, S., Musselwhite, D. & van der Laan, S. Melting processes in veined lithospheric mantle in cratonic and non-cratonic settings. In *International Kimberlite Conference: Extended Abstracts*, vol. 7, 220–223 (1998).

64. Green, D. H. *et al.* Experimental study of the influence of water on melting and phase assemblages in the upper mantle. *J. Petrol.* **55**, 2067–2096 (2014).

65. Downes, H. *et al.* Ultramafic xenoliths from the bearpaw mountains, montana, usa: Evidence for multiple metasomatic events in the lithospheric mantle beneath the wyoming craton. *J. Petrol.* **45**, 1631–1662 (2004).

66. Sun, S.-S. & McDonough, W. F. Chemical and isotopic systematics of oceanic basalts: implications for mantle composition and processes. *Geol. Soc. London, Special Publ.* **42**, 313–345 (1989).

67. Plank, T. & Langmuir, C. H. The chemical composition of subducting sediment and its consequences for the crust and mantle. *Chem. geology* **145**, 325–394 (1998).

68. Rudnick, R., Gao, S., Holland, H., Turekian, K. *et al.* Composition of the continental crust. *The crust* **3**, 1–64 (2003).

69. Mongelli, G., Paternoster, M., Rizzo, G., Sansone, M. T. C. & Sinisi, R. Trace element geochemistry of the mt vulture carbonatites, southern italy. *Int. Geol. Rev.* **55**, 1541–1552 (2013).

70. Downes, H. Formation and modification of the shallow sub-continental lithospheric mantle: a review of geochemical evidence from ultramafic xenolith suites and tectonically emplaced ultramafic massifs of western and central europe. *J. petrology* **42**, 233–250 (2001).

71. Liu, D. *et al.* Identifying mantle carbonatite metasomatism through os–sr–mg isotopes in tibetan ultrapotassic rocks. *Earth Planet. Sci. Lett.* **430**, 458–469 (2015).

72. Tumiati, S., Fumagalli, P., Tiraboschi, C. & Poli, S. An experimental study on coh-bearing peridotite up to 3· 2 gpa and implications for crust–mantle recycling. *J. Petrol.* **54**, 453–479 (2013).

73. Plank, T. Constraints from thorium/lanthanum on sediment recycling at subduction zones and the evolution of the continents. *J. Petrol.* **46**, 921–944 (2005).

74. Marschall, H. R. & Schumacher, J. C. Arc magmas sourced from mélange diapirs in subduction zones. *Nat. Geosci.* **5**, 862–867 (2012).

75. Wang, Y., Prelević, D. & Foley, S. F. Geochemical characteristics of lawsonite blueschists in tectonic mélange from the tavşanlı zone, turkey: potential constraints on the origin of mediterranean potassium-rich magmatism. *Am. Mineral. J. Earth Planet. Mater.* **104**, 724–743 (2019).

76. Wang, Y., Foley, S. F., Buhre, S., Soldner, J. & Xu, Y. Origin of potassic postcollisional volcanic rocks in young, shallow, blueschist-rich lithosphere. *Sci. Adv.* **7**, eabc0291 (2021).

77. Martin, L. H., Schmidt, M. W., Mattsson, H. B. & Guenther, D. Element partitioning between immiscible carbonatite and silicate melts for dry and h2o-bearing systems at 1–3 gpa. *J. Petrol.* **54**, 2301–2338 (2013).

78. Förster, M. W. *et al.* Sediment-peridotite reaction controls fore-arc metasomatism and arc magma geochemical signatures. *Geosciences* **11**, 372 (2021).

79. Förster, M. W. *et al.* Two-stage origin of k-enrichment in ultrapotassic magmatism simulated by melting of experimentally metasomatized mantle. *Minerals* **10**, 41 (2019).

80. Nikogosian, I. *et al.* Multiple subduction imprints in the mantle below italy detected in a single lava flow. *Earth Planet. Sci. Lett.* **449**, 12–19 (2016).

81. Ducea, M. N. *et al.* Diapirism of carbonate platforms subducted into the upper mantle. *Geology* (2022).

82. Shu, Z.-T. *et al.* Recycled carbonate-bearing silicate sediments in the sources of circum-mediterranean k-rich lavas: Evidence from mg-zn isotopic decoupling. *J. Geophys. Res. Solid Earth* e2022JB025135 (2023).

83. Rapp, R. P., Shimizu, N., Norman, M. & Applegate, G. Reaction between slab-derived melts and peridotite in the mantle wedge: experimental constraints at 3.8 gpa. *chemical Geol.* **160**, 335–356 (1999).

84. KEPEZHINSKAS, P. K., DEFANT, M. J. & DRUMMOND, M. S. Na metasomatism in the island-arc mantle by slab melt—peridotite interaction: evidence from mantle xenoliths in the north kamchatka arc. *J. Petrol.* **36**, 1505–1527 (1995).

Acknowledgements

We acknowledge the Scientific and Technological Research Council of Turkey (2219 Programme: International Postdoctoral Research Fellowship for Turkish Citizens) and the Deutsche Forschungsgemeinschaft (DFG, project PR 1072/9-1) for the financial support. We would like to thank Kathy Kuppers for her help with the preparation of the capsules.

Author contributions statement

F.G., D.P., S.B. and J.G. conceived the experiment(s); F.G., S.B. and J.G. conducted the experiment(s); F.G. and D.P. analysed the results; F.G and M.W.F made the calculations; F.G. and D.P. wrote and edited the text. All authors have read and reviewed the manuscript.

Additional information

The authors declare no competing interests.

Supplementary Material

Additional information on justification of the starting materials, capsule design and on mineral/melt compositions are covered in Supplementary Data File I. All mineral and melt analysis covered in Supplementary Data File II.

Data Availability

All data generated or analyzed during this study are included in this published article and its supplementary information files.

Supplementary Files

This is a list of supplementary files associated with this preprint. Click to download.

- SupplementaryDataFileI.pdf